ENGINEERING TRANSACTIONS • *Engng. Trans.* • **61**, 1, 15–31, 2013
Polish Academy of Sciences • Institute of Fundamental Technological Research (IPPT PAN)
National Engineering School of Metz (ENIM)

Parametric Study of Numerically Modelled Delamination Process in a Composite Structure Subjected to Dynamic Loading

Łukasz MAZURKIEWICZ, Krzysztof DAMAZIAK,
Jerzy MAŁACHOWSKI, Paweł BARANOWSKI

Military University of Technology
Faculty of Mechanical Engineering
Department of Mechanics and Applied Computer Science
Kaliskiego 2, 00-908 Warszawa, Poland
e-mail: {lmazurkiewicz, kdamaziak, jerzy.malachowski, pbaranowski}@wat.edu.pl

Composite materials, especially those fibre reinforced, thanks to their advantages, are being used in a growing number of industries. However, the complex structure of these materials results in many analytical problems. One such problematic field is to model failure of a composite, and especially the delamination process. The aim of this paper is to find a suitable method of layer connection modelling with the ability to describe delamination phenomena. A few chosen modelling parameters are investigated with respect to a parametric delamination numerical model.

Key words: fibre reinforced laminates (FRC), progressive crushing, cohesive modelling.

1. Introduction

Composite materials, particularly Fibre Reinforced Laminates (FRC), among other advantages are characterized by high specific strength and stiffness, weather resistance and increasingly lower costs of production. Elements made of composite materials also have high crashworthiness, which means that they are able to absorb a high amount of impact energy. Moreover, energy absorption can proceed in a controlled way [1, 2]. Thanks to its properties, composites make an excellent material for panels that reduce the effects of energy-intensive load due to outbreak acting on structural components [3]. However, to get the best energy-absorbing properties, it is necessary to conduct analyses of such panels to optimize its shape and internal layout, though the internal structure of FRC cause a number of modelling difficulties. Besides complex material properties, it is also very important to map destruction mechanisms of fibres and the matrix.

Due to the large amount of absorbed energy, the process of progressive crushing, where the main mechanism is delamination of the individual composite layers, is of particular interest. Since the analysis of elements made of FRC requires very complex modelling tools and, with the number of different coefficients included [4, 5], the influence of these coefficients on results and behaviour of the numerical model should be investigated. Because progressive crush phenomena are of particular interest in energy absorbing applications, the authors have focused their attention on several parameters related to delamination modelling.

Over recent decades, the modelling of progressive crush of FRC has attracted the attention of many researchers. Numerous modelling methods were developed in order to properly describe delamination phenomena. One of the most popular approaches is to use the so called decohesion material model. The cohesive-zone concept was originally introduced by Barenblatt [6] and Dugdale [7] (some authors also recognize the contribution of Leonov and Panasyuk [8]) to describe the near-tip fracture process, and it has gained great popularity as a tool for simulating delamination, debonding, fracture, and fragmentation, via the Finite Element Method (FEM). A body of publications showing this approach can be found. For instance, the authors of [9] reference around thirty of these. What should be noted though, is that only a few publications are available where the explicit simulation of progressive interface debonding were performed for a model with realistic geometry [10]. On the other hand, the application of composites for protection against outbreak requires quite large structural elements.

This paper shows one of the stages of research aimed to find the best way to include delamination in the simulation of real construction elements. Following some guidelines found in the literature, the very first FE models were made of shell elements (see Fig. 1a). Unfortunately, it so happens that this approach

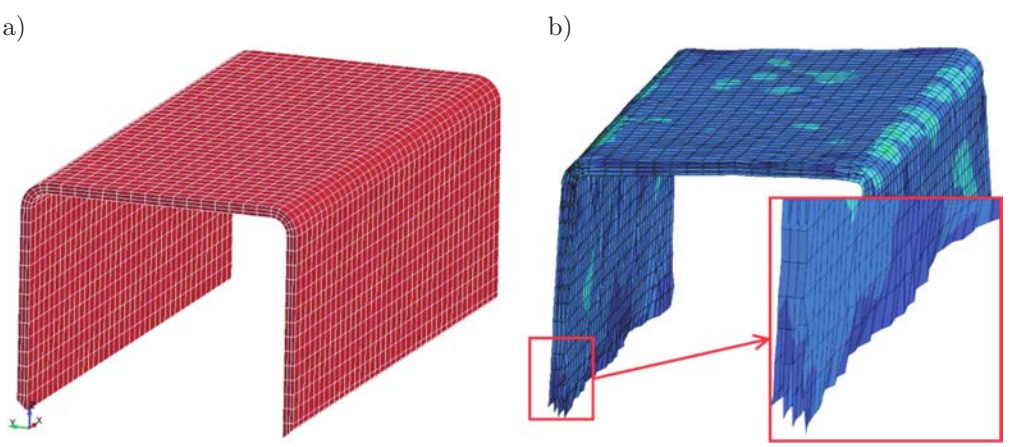

Fig. 1. a) Shell discreet model of FRC element; and b) instabilities in a non-loaded model.

leads to numerical instabilities. Despite changes in shell element formulation or element size, it was not possible to stabilize the solution. A typical symptom of instabilities is shown in Fig. 1b, where stress and deformation fields on the free (not loaded) structure are presented.

Due to the above problems, it was decided that the analysed structure would be modelled using 3D hexagonal elements and 2D interface cohesive elements. Keeping in mind the stability problems of 2D models, the authors decided to repeat numerical tests on a small coupon, which was used to identify material properties. Additionally, in order to verify the stability of the problem as an influence of some parameters on analysis of the results, a parametric study was carried out.

2. Research object

The research object is a rectangular coupon as shown in Fig. 2a. It is made of FRC (glass fibres) and has dimensions, 50 mm × 25 mm × 5 mm. It consists of four layers, each made of a fabric composed of four unidirectional layers with directions $0°/45°/90°/-45°$. One end of coupon has a 45° chamfer, which

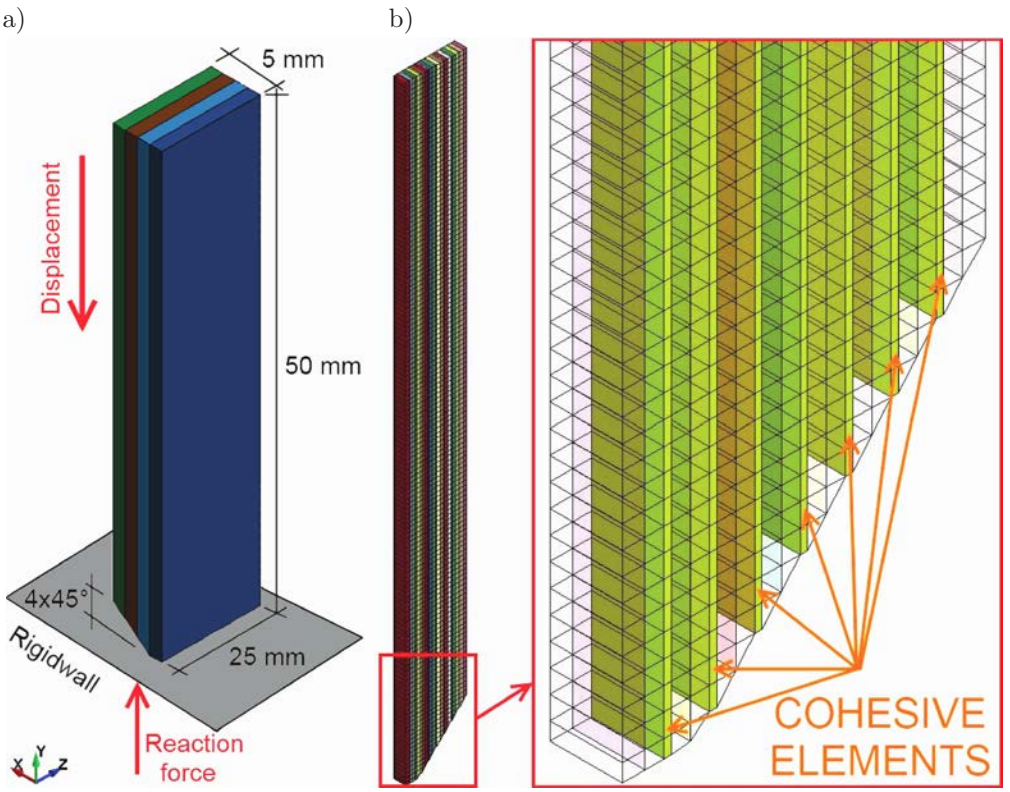

Fig. 2. a) Research object and b) discretisation of the research object.

serves as a delamination initiator. The FEM mesh is shown in Fig. 2b. Each layer was meshed using one row of hexagonal eight-node solid elements with one integration point. Layers were connected using eight-node cohesive interface elements.

Enforced motion along the y-axis was prescribed to the upper part of the coupon, while the bottom end impacted a rigid surface.

3. Constitutive model

Due to the nature of the investigated phenomena, the LS-Dyna explicit code was chosen as an analysis tool. From the number of composite material models available in the software, MAT_162 was chosen. This material model is specially designated to model failure mechanisms observed in composite materials consisting of unidirectional and woven fabric layers, and its usefulness was confirmed by the authors [11, 12].

3.1. Orthotropic material model for composite materials

In unidirectional laminates, the material properties are different along the fibre axis and along two other axes and thus the orthotropic material model is used in this research. The constitutive matrix is defined as [13]:

$$C^{-1} = \begin{bmatrix} \frac{1}{E_{aa}} & -\frac{\nu_{ab}}{E_{bb}} & -\frac{\nu_{ca}}{E_{cc}} & 0 & 0 & 0 \\ -\frac{\nu_{ab}}{E_{aa}} & \frac{1}{E_{bb}} & -\frac{\nu_{bc}}{E_{cc}} & 0 & 0 & 0 \\ -\frac{\nu_{ca}}{E_{aa}} & -\frac{\nu_{bc}}{E_{bb}} & \frac{1}{E_{cc}} & 0 & 0 & 0 \\ 0 & 0 & 0 & \frac{1}{G_{ab}} & 0 & 0 \\ 0 & 0 & 0 & 0 & \frac{1}{G_{bc}} & 0 \\ 0 & 0 & 0 & 0 & 0 & \frac{1}{G_{ca}} \end{bmatrix}, \tag{3.1}$$

where E_{aa}, E_{bb}, E_{cc}, G_{ab}, G_{bc}, G_{ca}, ν_{ab}, ν_{bc}, ν_{ca}, are material constants obtained from experimental tests.

The material layout with respect to the material axes is presented in Fig. 3.

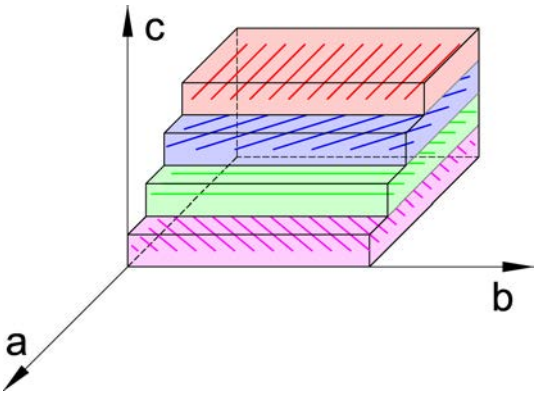

FIG. 3. Material directions.

3.2. Failure criteria for composite material

In the chosen material model layer, failure criteria have been established by adopting the methodology developed by Hashin [13] with a generalization to include the affect of highly constrained pressure on composite failure. The following failure criteria are available in the model [14]:

- Tensile/shear fibre failure mode

$$F_1 = \left(\frac{\sigma_a}{S_{aT}}\right)^2 + \left(\frac{\tau_{ab}^2 + \tau_{ca}^2}{S_{FS}^2}\right) - 1 = 0 \tag{3.2}$$

- Compression fibre failure mode

$$F_2 = \left(\frac{\sigma'_a}{S_{aC}}\right)^2 - 1 = 0, \qquad \text{where} \qquad \sigma'_a = -\sigma_a + \left(-\frac{\sigma_b + \sigma_c}{2}\right) \tag{3.3}$$

- Fibre crush failure mode

$$F_3 = \left(\frac{p}{S_{FC}}\right)^2 - 1 = 0, \qquad \text{where} \qquad p = \left(-\frac{\sigma_a + \sigma_b + \sigma_c}{3}\right) \tag{3.4}$$

- Perpendicular matrix mode

$$F_4 = \left(\frac{\sigma_b^+}{S_{bT}}\right)^2 + \left(\frac{\tau_{bc}}{S'_{bc}}\right)^2 + \left(\frac{\tau_{ab}}{S'_{ab}}\right)^2 - 1 = 0, \tag{3.5}$$

$$\text{where} \qquad S'_{bc} = S_{bc} + \tan(\varphi)\,(-\sigma_b)$$

- Parallel matrix mode

$$F_5 = \left(\frac{\sigma_c^+}{S_{cT}}\right)^2 + \left(\frac{\tau_{bc}}{S''_{bc}}\right)^2 + \left(\frac{\tau_{ca}}{S_{ca}}\right)^2 - 1 = 0, \tag{3.6}$$

$$\text{where} \qquad S''_{bc} = S_{bc} + \tan(\varphi)\,(-\sigma_c)$$

In the equations above, the indices a, b, c, denote directions in the material coordinate system, T and C stand for tension and compression, σ and τ are normal and shear stresses, and S are stress limits.

Static material properties were obtained from real-life tests (tension and compression in fibre and crossfibre directions, shearing in the planes 12, 23 and 31) and are shown in Table 1.

Table 1. Results of an experimental test of FRC.

Young modulus in tension (1)	E^t_{aa}	GPa	21.7
Young modulus in tension (2)	E^t_{bb}	GPa	605
Young modulus in compression (1)	E^c_{aa}	GPa	224
Young modulus in compression (2)	E^c_{bb}	GPa	748
Poisson (12)	ν_{ab}	–	0.19
Poisson (21)	ν_{ba}	–	0.099
Poisson (23)	ν_{bc}	–	0.40
Shear modulus (12)	G_{ab}	GPa	3.20
Shear modulus (21)	G_{ba}	GPa	224
Shear modulus (32)	G_{cb}	GPa	167
Tensile strength (1)	R^t_{aa}	MPa	402
Tensile strength (2)	R^t_{bb}	MPa	344
Compression strength (1)	R^c_{aa}	MPa	375
Compression strength (2)	R^c_{bb}	MPa	110
Shear strength (12)	S_{ab}	MPa	458
Shear strength (21)	S_{ba}	MPa	477
Shear strength (32)	S_{ca}	MPa	337
Tension failure strain (1)	e^t_{aa}		0.020
Tension failure strain (2)	e^t_{bb}	–	0.0065
Compression failure strain (1)	e^c_{aa}	–	0.017
Compression failure strain (2)	e^c_{bb}	–	0.020
Shear failure strain (12)	g_{ab}	–	> 0.05
Shear failure strain (21)	g_{ba}	–	> 005
Shear failure strain (32)	g_{ca}	–	0.019

Data provided by M. Klasztorny, P. Gotowicki, D. Nycz, Military University of Technology, Department of Mechanics and Applied Computer Science.

3.3. Cohesive interface constitutive model

Besides composite material data, additional input defining the cohesive interface has to be defined. Its traction-separation behaviour was given by energy

release rates for modes I and II, and peak traction in the normal and tangential directions (Fig. 4). A detailed description of this model can be found in [15].

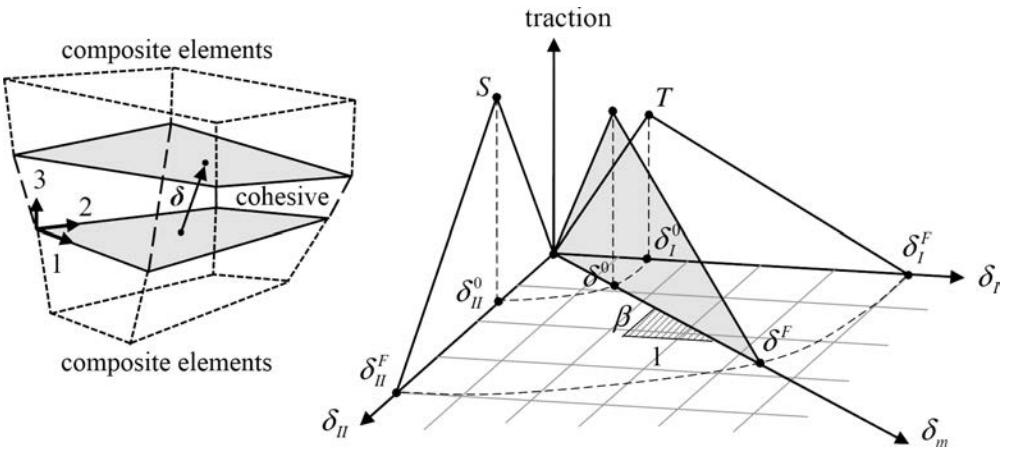

FIG. 4. Cohesive model used in analyses [15].

The ultimate mixed mode displacement is [15]:

$$\delta^F = \frac{1+\beta^2}{\delta^0}\left[\left(\frac{T}{G_{IC}}\right)^2 + \left(\frac{S\beta^2}{G_{IIC}}\right)^2\right]^{-1/2} \qquad \text{where} \quad \beta = \delta_{II}/\delta_I \tag{3.7}$$

and where T and S are ultimate stress in normal and tangential directions, δ_I and δ_{II} are the separation in normal and tangential directions, and G_{IC} and G_{IIC} are the release energies for models I and II.

4. Parametric studies

Initial analyses of coupon crushing showed that the FE model has a very different displacement pattern compared to the one seen in real-life tests. Since material data were taken from real-life tests, the cause of different numerical model behaviour has to lie in typical FE-related problems, such as an inadequate contact model, mesh density, etc. Therefore, a parametric study of the model was performed concerning:

- thickness of cohesive elements,
- mesh density and density of interface elements,
- contact stiffness (penalty stiffness factor),
- properties of cohesive elements (energy release rate and peak traction),
- and with respect to maximum crushing force.

Numerical analyses were performed using a transient dynamics procedure with explicit central difference time integration. The equations to be solved have the following form:

$$M\ddot{x}_n = F_n^{\text{ext}} - F_n^{\text{int}} - C\dot{x}_n \tag{4.1}$$

where M is the diagonal mass matrix, F_n^{ext} is the external and body force loads, F_n^{int} is the stress divergence vector, and C is the dumping matrix.

4.1. Thickness of cohesive elements

Three different thicknesses of cohesive elements were investigated: Case A – 0.00 mm, Case B – 0.01 mm, and Case C – 0.10 mm (see Fig. 5).

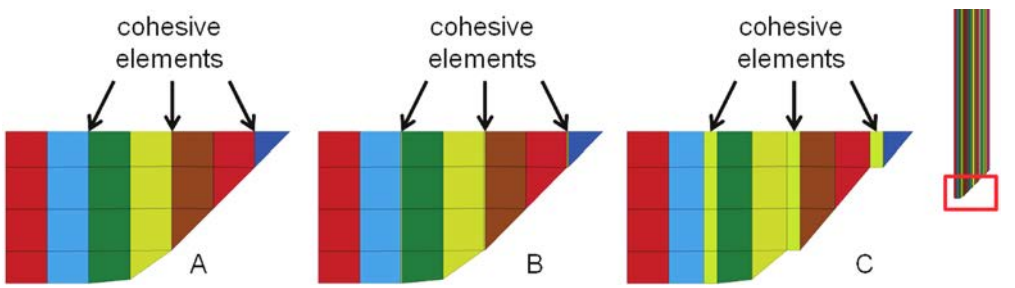

FIG. 5. Analysis cases – thickness of cohesive elements.

Displacement patterns are shown in Fig. 6. As one can see, Case A is numerically unstable, while Case C shows that the distance between composite layers is too big and, after separation (cohesive element failure), there is space allowing for artificial bending of layers.

The results obtained for Case B and Case C in terms of vertical force is shown in Fig. 7. It can be seen that the non-physical behaviour observed in the displacement pattern of Case C somehow does not strongly affect vertical force values.

The energy balance for Case B is presented in Fig. 8. The energy dissipated by cohesive elements has negative values (marked green). The internal energy of composite elements (red) is growing due to the deformation process and the total energy of the system is lower due to the process of dissipation.

The energy dissipated by the cohesive interface (Fig. 9) is significantly higher in Case B. This difference is caused by a different thickness of elements modelling composite layers, which was increased compared to Case C due to the reduced thickness of interface elements. Higher layer stiffness resulted in higher deformation of cohesive elements during coupon bending, since layers tended to separate instead of bend.

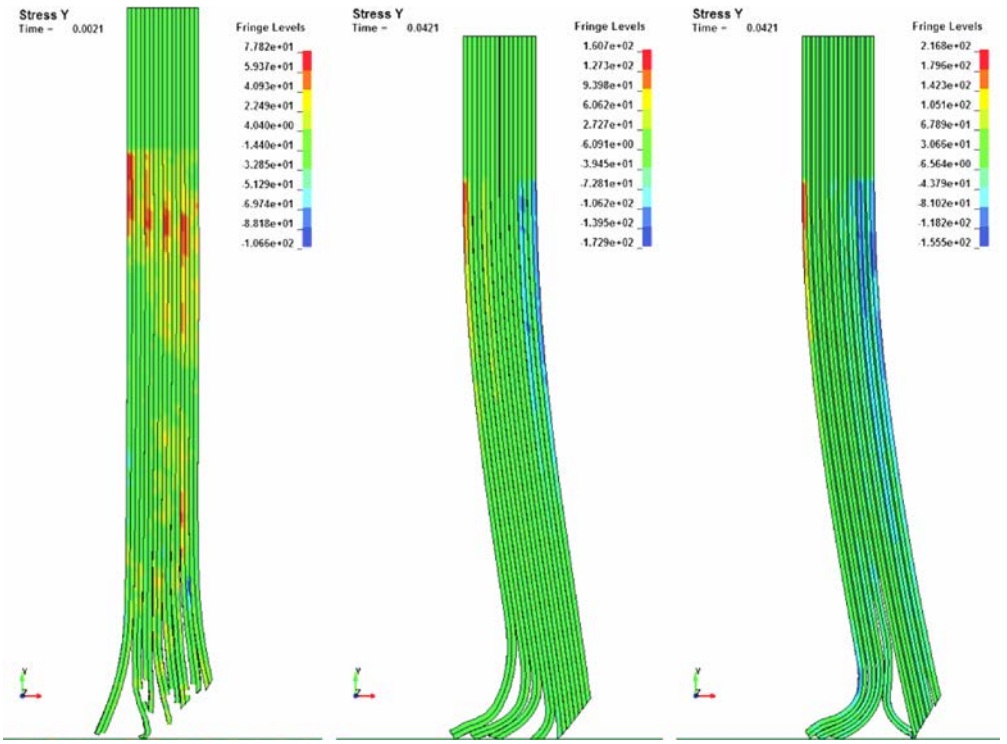

FIG. 6. Stress map and displacement of the models analysed (for model A, B and C, respectively).

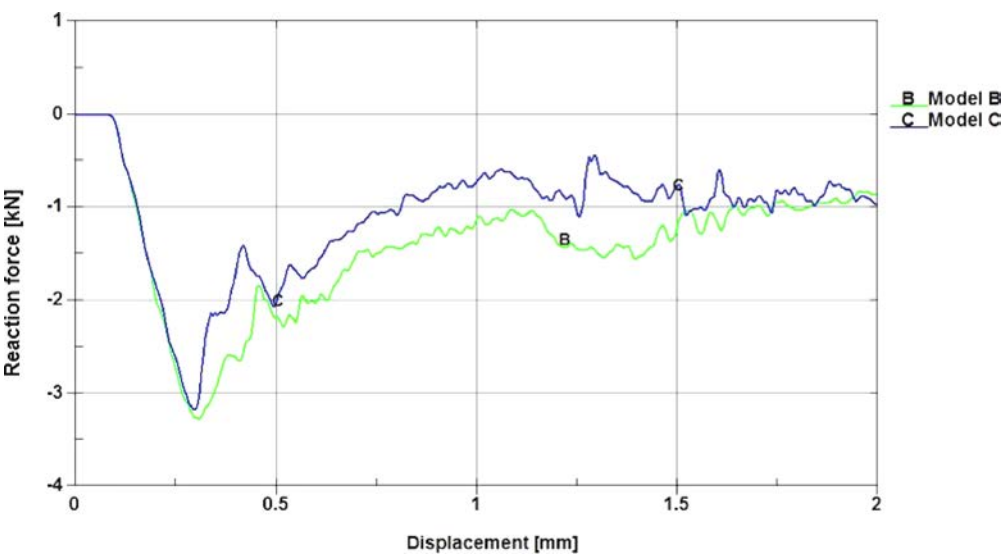

FIG. 7. Vertical force *versus* displacement for cases B and C.

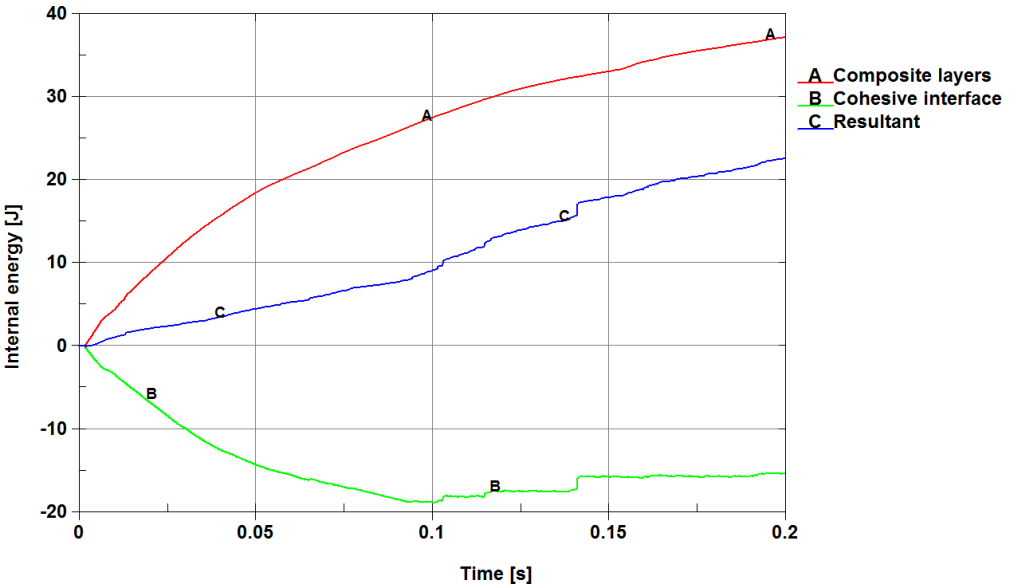

FIG. 8. Energy balance diagram.

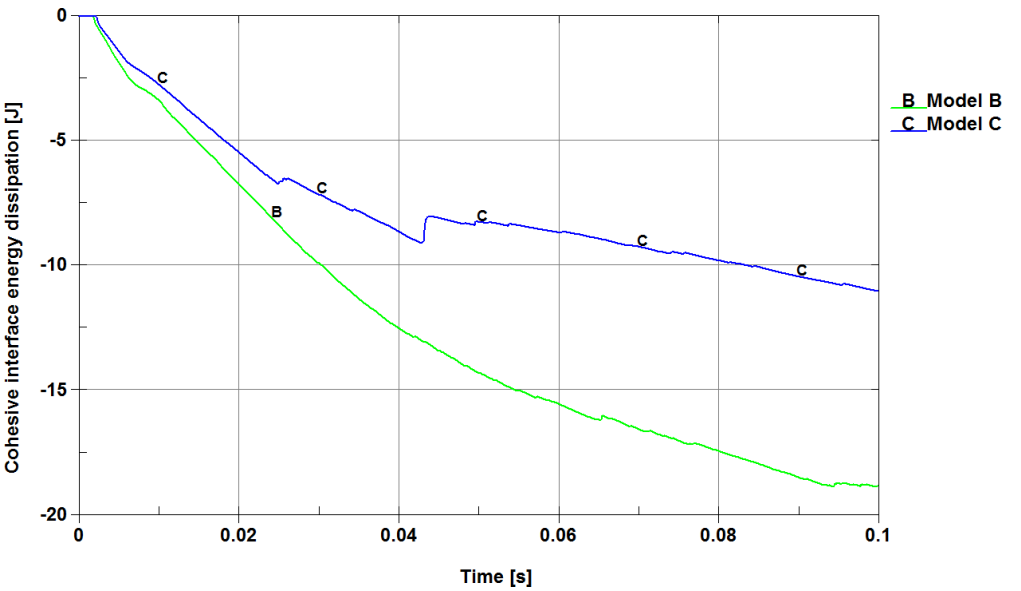

FIG. 9. Cohesive interface energy dissipation.

4.2. Mesh density

Three different FE models were built, as described in Table 2. The mesh layouts obtained are shown in Fig. 10.

Table 2. Analysis of cases in a mesh density parametric study.

	Case A	Case B	Case C
Number of solid elements per layer (composite) thickness	1 (16)	1 (16)	2 (32)
Number of cohesive elements per composite thickness	7	15	15

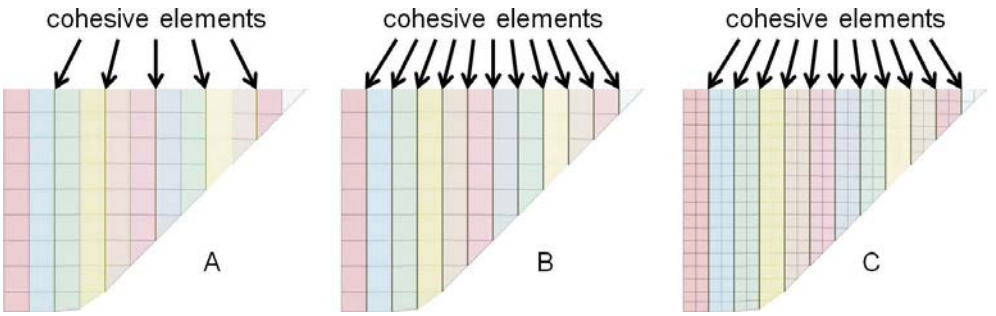

FIG. 10. Mesh layouts for the analysis of cases.

The deformed shapes of the model for all three cases are shown in Fig. 11. Once again it can be noted, that models with one element representing one

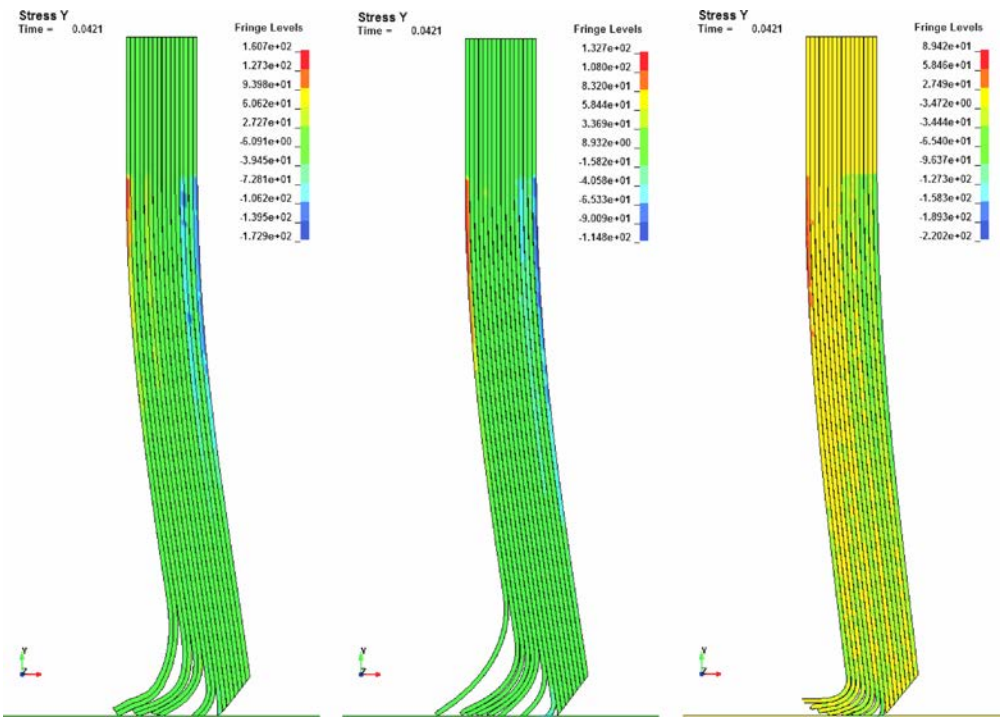

FIG. 11. Stress map and displacement of analysed models (respectively for model A, B and C according to Fig. 10).

layer are too stiff, preventing single layers from bending properly. This problem lays in the mathematical formulation of hexagonal elements with just one integration point as used in the examples presented. The usage of such simple elements is explainable and is because numerical analyses using explicit codes are always a trade off between integration speed and accuracy. Nevertheless, in the cases discussed, the low quality of elements obviously affected the results obtained.

The response of the models, with respect to vertical force is shown in Fig. 12. The curves obtained confirm the observation made based on deformation shapes. Case C, with two elements per layer, is less stiff than the other two.

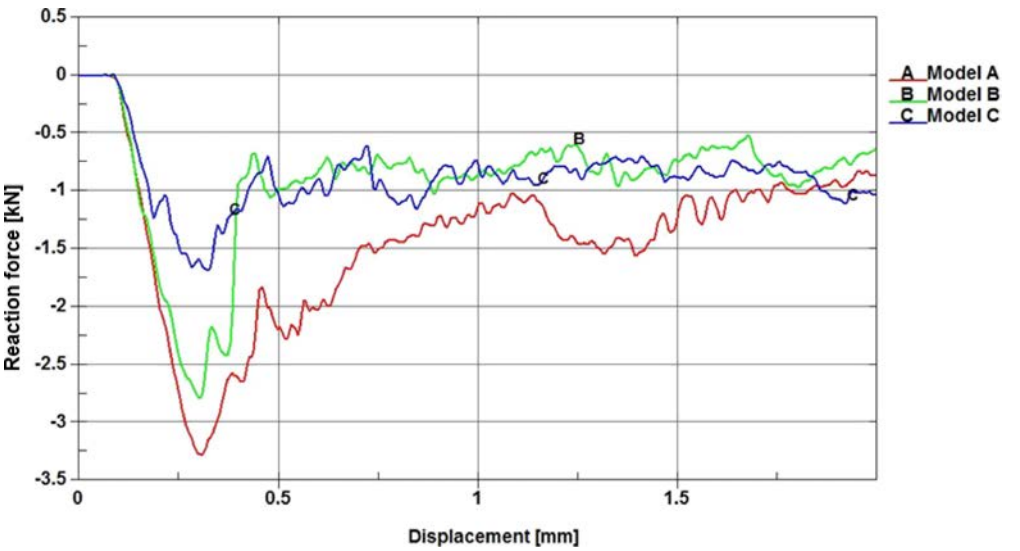

FIG. 12. Vertical force as a function of displacement for the analysed models.

The addition of cohesive interfaces (more delamination planes) in Model B result in higher energy being dissipated by that interface, as compared to Model A (Fig. 13).

The usage of a thickness of two elements per layer (Case C) allow a better description of bending, which result in lower stress values in the coupon and a more even load of cohesive elements. Model B is too stiff, which leads to the development of negative X stress components in the middle part of the coupon. These stresses prevent cohesive elements from opening. As a result, the dissipated energy is significantly smaller than in the case of the more flexible Model C.

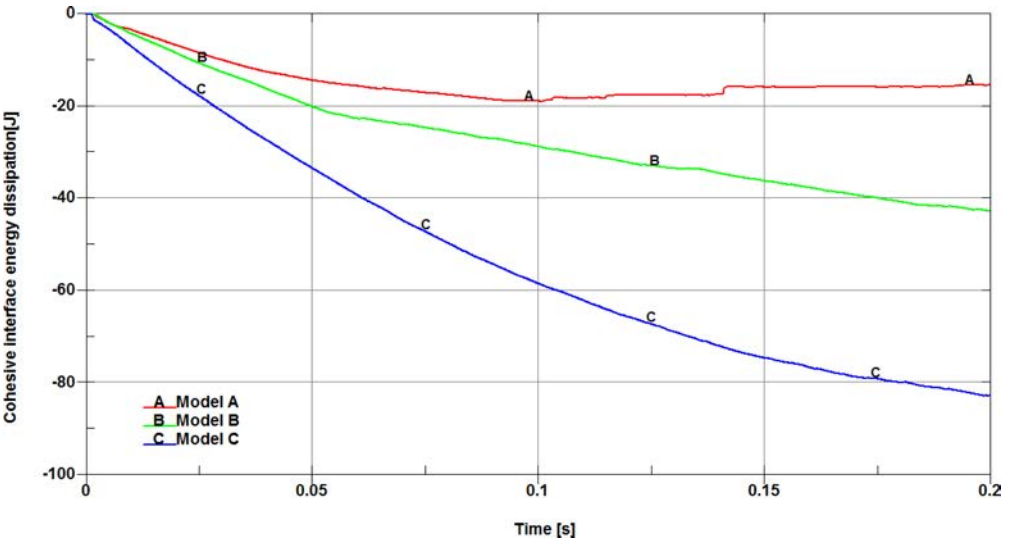

FIG. 13. Cohesive interface energy dissipation.

4.3. Contact stiffness

The next parameter investigated was contact stiffness. The implemented contact formulation is based on a penalty function approach. In segment based contact, stiffness is described as follows:

$$k_{cs} = 0.5 SLSFAC \left\{ \begin{array}{c} SFS \\ \text{or} \\ SFM \end{array} \right\} \left(\frac{m_1 m_2}{m_1 + m_2} \right) \left(\frac{1}{\Delta t_c\,(t)} \right)^2, \tag{4.2}$$

where $SLSFAC$ is a scaling factor for sliding interface penalties, SFS is a scaling factor for slave penalty stiffness, SFM is a scaling factor for master penalty stiffness, and m_1 and m_2 are the masses of slave and master segments.

The stiffness factors SFS and SFM were changing in two contact interfaces:

- between base and composite – from 0.001 to 2,
- and between composite layers – from 0.001 to 2.

The results obtained are shown in Fig. 14. As can be seen, the penalty value in contact interfaces has no real influence on the vertical force, but very low values of contact stiffness between the base and composite cause a failure of the contact algorithm. The coupon model has penetrated through the base surface.

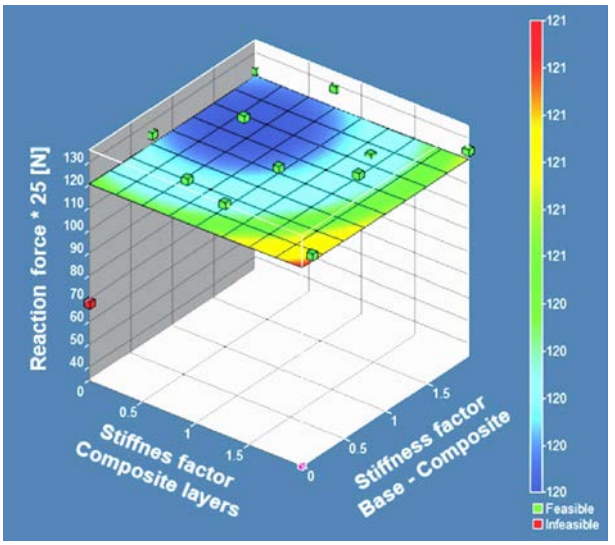

FIG. 14. Response surface of crushing force as a function of contact stiffness factors.

4.4. Cohesive stiffness

The last parameter to be checked is the stiffness of cohesive elements. One particular reason to perform such study was to learn parametric of FE model on possible errors in G_I or G_{II} estimates. This time, the variable parameters were (see Fig. 15):

- energy release rate, $G_{IC} = 0.01 \div 10$ J/mm^2 and $G_{IIC} = 5G_{IC}$,
- and peak traction in normal and tangential directions, $T = 5 \div 100$ MPa and $S = 2$ T.

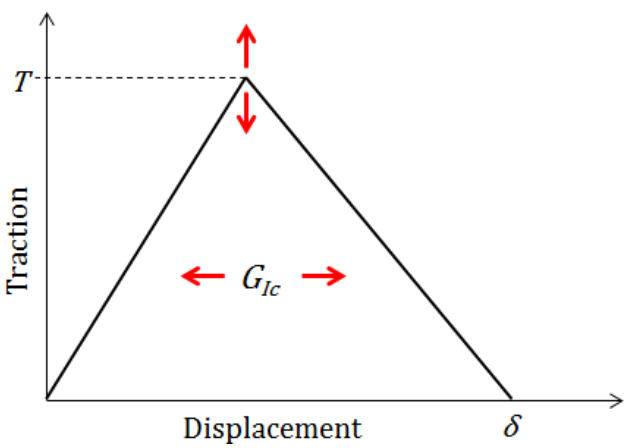

FIG. 15. Traction-separation curve for cohesive elements with red arrows representing changes in the variables.

The results of the analyses are shown on Fig. 16. It can be seen that the coupon FE model is very sensitive to changes in cohesive material properties as far as to make the numerical model unstable (higher values of energy release rates cause shear locking).

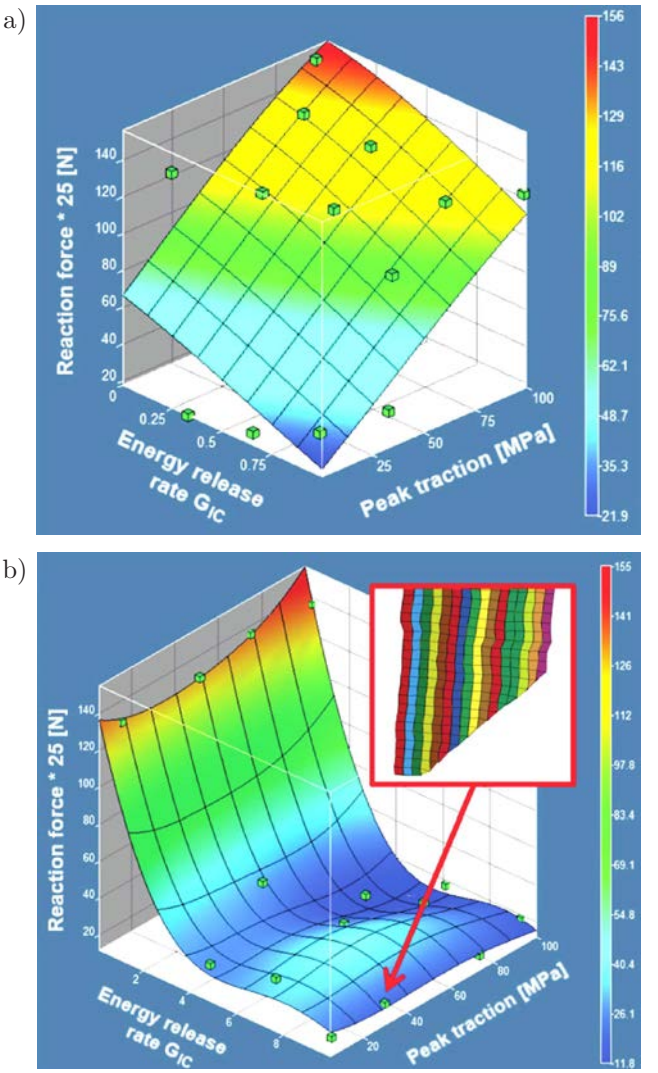

FIG. 16. Response surface of crushing force as a function of energy release rate and peak traction: a) $G_{IC} = 0.01 \div 1$ J/mm^2; and b) $G_{IC} = 0.1 \div 10$ J/mm^2.

5. Results discussion and conclusions

One of the most important conclusions is that numerical modelling of progressive crush phenomena is very challenging. Despite the fact that the cohesive

material model is well established, it is quite difficult to conduct a stable analysis of the process. Additionally, the internal structure of FRC has to be adequately described, which leads to very large and complicated FE models.

Typical limitations of (or rather, incorrect use of) the FE approach manifest themselves during tests. A too large thickness of interface elements leads to the generation of an artificial space between composite layers, which lead to nonphysical behaviour of layers after delamination. An insufficient number of elements-per-layer thickness makes that a single layer is too stiff for bending.

An analysis of the results obtained show that most of the investigated parameters do not greatly affect the crushing force value, with the exception of energy release rates. This means, that just like other material data, G_I, G_{II}, and traction need to be accurately acquired. Therefore, material data taken from literature should be treated as preliminary data only. At the moment, the authors are carrying out real-life tests in order to obtain the fracture toughness of FRC. This means that both the experimental stages of material data acquisition as well as the FE analyses are very laborious and time consuming as far as the lack of usability in the case of modelling real objects is concerned.

Acknowledgment

The research was carried out under a research grant from the Polish Ministry of Science and Higher Education, no. 0097/R/T00/2010/12. This support is gratefully acknowledged.

References

1. Ochelski S., Bogusz P., Kiczko A., *Static axial crush performance of unfilled and foamed-filled composite tubes*, Bulletin of the Polish Academy of Sciences Technical Sciences, **60**, 1, 31–35, 2012.
2. Zangani D., Robinson M., Gibson A.G., *Progressive Failure of Composite Hollow Sections with Foam-Filled Corrugated Sandwich Walls*, Appl. Compos. Mater., **14**, 325–342, 2007.
3. Tekalur S.A., Shukla A., Shivakumar K., *Blast resistance of polyurea based layered composite materials*, Composite Structures, **84**, 271–281, 2008.
4. Gama B.A., Gillespie J.W. Jr., *Finite element modeling of impast, damage evolution and penetration of thick-section composites*, International Journal of Impact Engineering, **38**, 181–197, 2011.
5. Xiao J.R., Gamma B.A., Gillespie J.W. Jr., *Progressive damage and delamination in plain weave S-2 glass/SC-15 composites under quasi-static punch-shear loading*, Composite Structures, **78**, 182–196, 2007.
6. Barenblatt G.I., *The formation of equilibrium cracks during brittle fracture: general ideas and hypotheses axially symmetric cracks*, Appl. Math. Mech., **23**, 622–36, 1959.

7. Dugdale D.S., *Yielding of steel sheets containing slits*, J. Mech. Phys. Solids, **8**, 100–4, 1960.

8. Leonov M.Y., Panasyuk V.V., *The micro cracks development in a solid* [in Ukrainian], Prikladnaya Mekhanika, **5**, 391–401, 1959.

9. Valoroso N., Champaney L., *A damage-mechanics-based approach for modelling decohesion in adhesively bonded assemblies*, Engineering Fracture Mechanics, **73**, 2774–2801, 2006.

10. Sevkat E., Liaw B., Delale F., Raju B.B., *A combined experimental and numerical approach to study ballistic impact response of S2-glass fiber/toughened epoxy composite beams*, Composites Science and Technology, **69**, 965–982, 2009.

11. Hufenbach W., Langkamp A., Hornig A., Zscheyge M., Bochynek R., *Analysing and modelling the 3D shear damage behaviour of hybrid yarn textile-reinforced thermoplastic composites*, Composite Structures, **94**, 121–131, 2011.

12. Kushch V.I., Shmegera S.V., Mishnaevsky L. Jr., *Explicit modeling the progressive interface damage in fibrous composite: Analytical vs. numerical approach*, Composites Science and Technology, **71**, 989–997, 2011.

13. Hashin Z., *Failure Criteria for Unidirectional Fiber Composites*, J. Appl. Mech., **47**, 2, 329–335, 1980.

14. *LS-Dyna Keyword User's Manual Volume I*, February 14, 2012 (revision: 1197), Version 971, Livermore Software Technology Corporation (LSTC).

15. Gerlach S., Fiolka M., Matzenmiller A., *Modelling and analysis of adhesively bonded joints with interface elements for crash analysis*, Konferenzbeitrag zum 4. LS-DYNA FORUM, Bamberg, DYNAmore GmbH, Stuttgart, October 20–21, 2005.

16. Hallquist J.O., *LS-Dyna Theory manual*, March 2006, Livermore Software Technology Corporation (LSTC).

Received May 25, 2012; revised version November 27, 2012.